

# Picroside II prevents HSC activation and liver fibrosis in Mdr2<sup>-/-</sup> mice by polarizing M1 macrophages and balancing immune responses

Kexin Jia<sup>1</sup>, Zhi Ma<sup>1</sup>, Yinhao Zhang<sup>1</sup>, Jianzhi Wu<sup>1</sup>, Xiaoyong Xue<sup>1</sup>, Runping Liu<sup>1</sup>, Jiaorong Qu<sup>1</sup>, Fanghong Li<sup>1</sup>, and Xiaojiaoyang Li<sup>1</sup>

<sup>1</sup>Beijing University of Chinese Medicine

April 27, 2023

## Abstract

**Background and Purpose:** Macrophages are central immune characters in hepatic fibrosis by reconstructing the fibrotic immune microenvironment. Picroside II (PIC II) has exerted a therapeutic potential on liver injury. However, the mechanisms by which macrophage initiates immune cascades and further contributes to liver fibrosis and whether this process can be influenced by PIC II remains unclear. **Experimental Approach:** In this research, the RNA sequencing of multidrug-resistance protein 2 knockout (Mdr2<sup>-/-</sup>) mice was applied. Then aHSCs were incubated with the medium from M1 macrophages and NK cells, with the extra formation of neutrophils extracellular traps (NETs) being tested. In addition, we intraperitoneal injected PIC II and then intravenously injected the clodronate liposome to evaluate the therapeutic effect of PIC II and macrophage deletion in Mdr2<sup>-/-</sup> mice. **Key Results:** We observed the increase of CXCL16+ M1 macrophages in Mdr2<sup>-/-</sup> liver, accompanied by the recruitment of CXCR6+ NK cells and NETs formation. PIC II promoted the CXCL16+ macrophage recruited NK cells via CXCL16/CXCR6 axis, which subsequently affecting the JAK1/STAT1 signaling in aHSCs. And fibrotic liver was relieved to some extent when PIC II combined with macrophage depletion. **Conclusion and Implications:** Mechanistically, PIC II activated M1 macrophage to recruit NK cells via CXCL16-CXCR6 axis and subsequently regulated the JAK1/STAT1 signaling to restrain aHSCs. PIC II also alleviated fibrosis by attenuating the formation of NETs. Notably, these PIC II-associated hepatoprotective effects were largely reversed by macrophage depletion in Mdr2<sup>-/-</sup> mice. Collectively, our research suggests that PIC II is potential for halting the liver fibrosis.

**Title: Picroside II prevents HSC activation and liver fibrosis in Mdr2<sup>-/-</sup> mice by polarizing M1 macrophages and balancing immune responses**

**Short title: Picroside II prevents liver fibrosis via modulating immune microenvironment**

Kexin Jia<sup>1</sup>, #, Zhi Ma<sup>1</sup>, #, Yinhao Zhang<sup>1</sup>, Jianzhi Wu<sup>1</sup>, Xiaoyong Xue<sup>1</sup>, Runping Liu<sup>2</sup>, Jiaorong Qu<sup>1</sup>, Fanghong Li<sup>2</sup>, Xiaojiaoyang Li<sup>1</sup>, \*

<sup>1</sup> School of Life Sciences, Beijing University of Chinese Medicine, Beijing, 100029, China

<sup>2</sup> School of Chinese Materia Medica, Beijing University of Chinese Medicine, Beijing, 100029, China

#**These authors contributed equally to this work.**

\***Corresponding authors:** Prof. Xiaojiaoyang Li

**Address correspondence to:**

Xiaojiaoyang Li, Ph.D.

School of Life Sciences

Beijing University of Chinese Medicine, Beijing, China

Email: [xiaojiaoyang.li@bucm.edu.cn](mailto:xiaojiaoyang.li@bucm.edu.cn)

**Acknowledgment:** This work was supported by grants from National Key Research and Development Program on Modernization of Traditional Chinese Medicine (NO. 2022YFC3502100 to XL); National Natural Science Foundation of China (Grant NO. 82274186 to XL); the National High-Level Talents Special Support Program to XL; Young Talents Promotion Project of China Association of Traditional Chinese Medicine (Grant NO. 2020-QNRC2-01 to XL); Innovation Team and Talents Cultivation Program of National Administration of Traditional Chinese Medicine (Grant NO. ZYYCXTD-C-202006 to XL).

**Conflict of interest statement:** The authors report no conflicts of interest. The authors alone are responsible for the content and writing of this article.

## Abstract

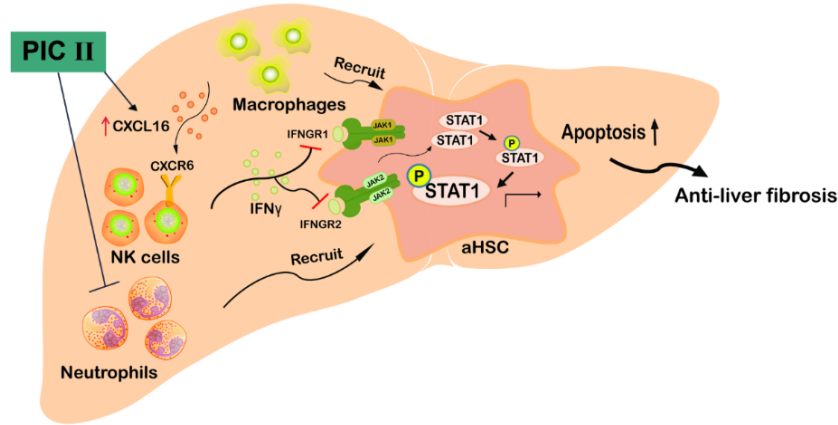
**Background and Purpose:** Macrophages are central immune characters in hepatic fibrosis by reconstructing the fibrotic immune microenvironment. Picoside II (PIC II) has exerted a therapeutic potential on liver injury. However, the mechanisms by which macrophage initiates immune cascades and further contributes to liver fibrosis and whether this process can be influenced by PIC II remains unclear.

**Experimental Approach:** In this research, the RNA sequencing of multidrug-resistance protein 2 knockout ( $Mdr2^{-/-}$ ) mice was applied. Then aHSCs were incubated with the medium from M1 macrophages and NK cells, with the extra formation of neutrophils extracellular traps (NETs) being tested. In addition, we intraperitoneal injected PIC II and then intravenously injected the clodronate liposome to evaluate the therapeutic effect of PIC II and macrophage deletion in  $Mdr2^{-/-}$  mice.

**Key Results:** We observed the increase of  $CXCL16^{+}$  M1 macrophages in  $Mdr2^{-/-}$  liver, accompanied by the recruitment of  $CXCR6^{+}$  NK cells and NETs formation. PIC II promoted the  $CXCL16^{+}$  macrophage recruited NK cells *via*  $CXCL16/CXCR6$  axis, which subsequently affecting the JAK1/STAT1 signaling in aHSCs. And fibrotic liver was relieved to some extent when PIC II combined with macrophage depletion.

**Conclusion and Implications:** Mechanistically, PIC II activated M1 macrophage to recruit NK cells *via*  $CXCL16-CXCR6$  axis and subsequently regulated the JAK1/STAT1 signaling to restrain aHSCs. PIC II also alleviated fibrosis by attenuating the formation of NETs. Notably, these PIC II-associated hepatoprotective effects were largely reversed by macrophage depletion in  $Mdr2^{-/-}$  mice. Collectively, our research suggests that PIC II is potential for halting the liver fibrosis.

**Keywords:** Liver fibrosis; picoside II; M1 macrophage; hepatic stellate cell; natural killer cell; neutrophil;  $CXCL16$ .



## Graphical Abstract

**Keywords:** Liver fibrosis; picoside II; M1 macrophage; hepatic stellate cell; natural killer cell; neutrophil; CXCL16.

**Abbreviation:** ALT, alanine aminotransferase; AST, aspartate aminotransferase; AKP, alkaline phosphatase; CL, clodronate liposome; Col1a1, collagen type I alpha I chain; Csf3r, colony-stimulating factor 3 receptor; CM, culture medium; CXCL16, C-X-C motif chemokine ligand 16; CXCR6, C-X-C motif chemokine receptor 6; ECM, extracellular matrix; GZMB, granzyme B; HSC, hepatic stellate cell; IFN- $\gamma$ , interferon-gamma; IL-2, interleukin-2; JAK1, Janus kinase 1; Mdr2, multidrug resistance protein 2; MMP2, matrix metalloproteinase 2; MPO, myeloperoxidase; NETs, neutrophil extracellular traps; PSC, primary sclerosing cholangitis; PIC II, picoside II; STAT, signal transducer and activator of transcription; TBA, total bile acid; TGF- $\beta$ , transforming growth factor- $\beta$ ; Timp1, tissue inhibitor of metalloproteinase 1; TRAIL, tumor necrosis factor-related apoptosis-inducing ligand; WGCNA, weighted gene co-expression network analysis;  $\alpha$ -SMA,  $\alpha$ -smooth muscle actin.

## Introduction

Hepatic fibrosis is a complex pathological process of recurrent inflammation induced by various hepatic injuries and is characterized by fibrous scar formation, due to the dysregulated overproduction and gradual excessive accumulation of excessive extracellular matrix (ECM) (Parola & Pinzani, 2019). If get out of control, this process may continue to deteriorate severe liver diseases such as cirrhosis and hepatocellular carcinoma. Throughout the entire process, inflammatory reactions triggered by hepatocellular injury or necrosis of hepatic parenchymal or non-parenchymal cells are the major risk factors for the initiation and development of liver fibrosis, since the infiltration of inflammatory immune cells and their released chemotactic peptides may interact with each other and finally amplify the reaction of hepatic stellate cell (HSC) activation (Ma et al., 2017). To break through the bottleneck of anti-fibrosis drug development, ocaliva, an agonist of the nuclear receptor farnesoid X receptor (FXR) that emerged as a vital regulator in hepatic fibrosis, has been approved by the FDA for the treatment of biliary fibrosis. However, its side effects including but not limited to, pruritus, fatigue, abdominal pain, immunologic derangement, dizziness, and even in severe cases, acute liver failure, have restricted its popularization and application (Shah & Kowdley, 2020). Hence, there is an urgent need to explore the pathogenesis and specific targets of novel drugs for alleviating liver fibrosis.

The deficiency of multidrug resistance protein 2 (Mdr2) protein, a crucial transport protein closely associated with bile secretion, is reported to result in the accumulation of toxic bile acids and subsequent hepatocyte and cholangiocyte injuries, effectively mimicking the clinical pathological characteristics in primary sclerosing cholangitis (PSC) (Liu et al., 2020; Ma et al., 2017). Additionally, the Mdr2 knockout (Mdr2<sup>-/-</sup>) mouse is

a well-known fibrotic mouse model and has been widely used for investigating the pathogenesis of liver fibrosis and evaluating drug efficacy (Liu et al., 2019). Targeting inflammatory pathways or influencing immune cells in anti-fibrotic therapies is promising in recent years. Especially, M1- and M2-like monocyte-derived macrophages have been demonstrated to be tightly associated with sclerosing cholangitis in *Mdr2*<sup>-/-</sup> mice by means of chemokines like CCL2-CCR2/CCR5 axis and FXR-related pathways, reminding us that abnormal changes of macrophages are not only features but also indispensable initial participants of hepatic fibrosis (Guicciardi et al., 2018; Shi et al., 2022). Gevitha *et al.* focused on how the absence of interferon-gamma (IFN- $\gamma$ )-mediated signaling shaped the production of chemokines and immune cell recruitment, and ultimately influenced liver fibrotic in *Mdr2*<sup>-/-</sup> mice model. They also confirmed that the increase of IFN- $\gamma$  promotes the expression of granzyme B (GZMB) and tumor necrosis factor-related apoptosis-inducing ligand (TRAIL) from CD8<sup>+</sup> T and natural killer (NK) cells, further resulting in the inhibition of activated hepatic stellate cells (aHSCs) and the remission of liver fibrosis (Ravichandran et al., 2019). Besides, low doses of interleukin-2 (IL-2) upregulated the expression of CD39 in T regulatory cells to inhibit the hepatic CD8<sup>+</sup>lymphocyte proliferation, further leading to diminished fibrosis in *Mdr2*<sup>-/-</sup> mice (Taylor et al., 2018). However, the potential mechanisms of pathological transformation from hepatic inflammation to fibrosis and complex crosstalk between multiple immune cells especially for macrophages and NK cells that lead to hepatic fibrosis in *Mdr2*<sup>-/-</sup> mice have not been fully elucidated.

Picroside II (PIC II), one of the representative active components of the *Picrorhizae rhizoma*, has been demonstrated to exert a therapeutic potential on ischemia/reperfusion injury, liver damage, and organic cancer metastasis through inhibiting inflammation, oxidative stress and angiogenesis (Li et al., 2020; Ma et al., 2020). In recent years, researchers have gradually turned their attention on the hepatic protective role and immunoregulative function of PIC II. In the alpha-naphthyliso thiocyanate-induced cholestasis mice model, PIC II significantly activated FXR to regulate the activities of bile acid efflux transporters and bile acid metabolizing enzymes in livers (Li et al., 2020). Meanwhile, bile acids were reported to have a potential effect in regulating the whole-body immune system *via* influencing the balance of gut microbiome or inducing signal transduction as messengers (Duan et al., 2022), which reminds us PIC II might possess a direct influence on disparate immune cells in the liver. Meanwhile, although there is no direct regulatory effect on immune cells, PIC II could alleviate apoptosis and inflammation in sepsis by decreasing the expression of toll-like receptor 4 (TLR4) and tumor necrosis factor-alpha (TNF $\alpha$ ) in an ischemic injured rat model (Huang et al., 2016). Of note, PIC II also inhibited NF- $\kappa$ B activation and achieved the alleviation of inflammatory response and apoptosis in endotheliocytes by regulating the sirtuin 1 (SIRT1)/lectin-like oxLDL receptor-1 (LOX-1) signaling pathway (Wang et al., 2019). However, whether PIC II was able to protect the liver from *Mdr2* deficiency-induced liver fibrosis and the potential interaction between the PIC II and different immune cells in fibrotic livers still needs to be clarified.

In the current study, we aimed to systematically investigate the pathological role of multiple immune cells involved in *Mdr2* deficiency-induced liver fibrosis and to explore whether PIC II could achieve its hepatoprotective effects by influencing the function of and interaction between different immune cells in the fibrotic liver. Our findings not only evaluate how different immune cells regulate the immune microenvironment and HSCs activation during the development of liver fibrosis, but also offered a kind of natural ingredients as a novel therapeutic option for removing the bottleneck of antifibrosis.

## Methods and materials

### 2.1 Materials

PIC II (PS0323) was obtained from PUSH BIO-Technology (Chengdu, China). Mouse IL-2, mouse transforming growth factor- $\beta$  (TGF- $\beta$ ) and mouse IFN- $\gamma$  (C746) were purchased from Novoprotein Co., Ltd. (Shanghai, China). Lipopolysaccharide (LPS) and other consumables were obtained from Sigma-Aldrich (St. Louis, USA). Antibodies against F4/80 (28463-1-AP), collagen 1 (COL, *Col1a1*) (67288-1-AP), fibronectin (FN, *Fn1*) (15613-1-AP), C-X-C motif chemokine ligand 16 (CXCL16 (60123-1-Ig), myeloperoxidase (MPO) (66177-1-Ig), Janus kinase 1 (JAK1) (66466-1-Ig), tyrosine kinase 2 (TYK2) (67411-1-Ig), PERFORIN (14580-1-AP), GZMB (13588-1-AP), CD11B (66519-1-Ig) and  $\beta$ -Actin (66009-1-Ig) were ob-

tained from Proteintech (Rosemont, USA). Antibodies against histone H3 (citrulline R2/R8/R17) (ab5103) and CD161 (ab197979) were purchased from Abcam (Cambridge, USA). Antibody against  $\alpha$ -smooth muscle actin ( $\alpha$ -SMA,  $\alpha$ -SMA) (19245S) was obtained from Cell Signaling Technology (Danvers, USA). Antibodies against signal transducer and activator of transcription 1 (STAT1) (A12075), p-STAT1 (AP0453), p-JAK1 (AP0530), p-TYK2 (AP0543) and CD68 (A13286) were purchased from ABclonal Technology Co.,Ltd. (Wuhan, China). Antibody against CXCR6 (E-AB-11112) was obtained from Elabscience Biotechnology Co.,Ltd (Wuhan, China). Alexa Fluor 594 anti-rabbit IgG secondary antibody (8889S) was purchased from Cell Signaling Technology (Danvers, USA), and Alexa Fluor 488 anti-mouse IgG secondary antibody (A32723) was obtained from Thermo Fisher Scientific (Waltham, USA).

## 2.2 Animal studies

Mdr2<sup>-/-</sup> mice (7 weeks old, 20-22 g, male and female) were housed and maintained under specific pathogen-free conditions in a standard environment with a 12-hour light-dark cycle and fed a diet of normal chow *ad libitum*. All animal studies and procedures were sanctioned by the Institutional Animal Care and Use Committee of Beijing University of Chinese Medicine and performed in compliance with all guidelines and regulations. After acclimatization for 1 week, mice were randomly divided into 4 groups (n = 6): (1) wild type (WT) group; (2) Mdr2<sup>-/-</sup> group; (3) Mdr2<sup>-/-</sup> + PIC II low dose (L) group (5 mg/kg); (4) Mdr2<sup>-/-</sup> + PIC II high dose (H) group (10 mg/kg). Mice in group (1) and (2) were given saline and mice in groups (3)-(4) were administrated with two different doses of PIC II for 14 days. In the macrophage depletion experiment, mice were randomly divided into 4 groups (n = 6): (1) WT group; (2) Mdr2<sup>-/-</sup> + empty liposome (Neg) group; (3) Mdr2<sup>-/-</sup> + clodronate liposome (CL) group; (4) Mdr2<sup>-/-</sup> + CL + PIC II group (10 mg/kg). Mice in group (2) were given empty liposome and mice in groups (3)-(4) were administrated with clodronate-liposomes (1 mg/ml, 50  $\mu$ l/mouse, YEASEN, Shanghai, China) through tail vein once every three days until the day before sacrificed. Mice in group (4) were also administrated with 10 mg/kg PIC II for 14 days. After treatment, all mice in different groups were sacrificed to obtain blood and liver samples for following experiments.

## 2.3 Histological and immunofluorescence staining

After fixation in formalin for one week, the livers were embedded in paraffin and cut into 4.5  $\mu$ m thick sections for subsequent staining. After deparaffinization in xylene and dehydration in ethanol, the sections were stained using a hematoxylin and eosin (H & E) staining kit and a Masson's staining kit. For immunofluorescence, the sections were blocked with 0.2% Triton X-100-2.5% BSA-1  $\times$  phosphate-buffered saline (PBS)-10% goat serum after subjecting to antigen retrieval solution. The primary antibodies against FN (dilution 1:200),  $\alpha$ -SMA (dilution 1:400), COLLAGEN (dilution 1:400), F4/80 (dilution 1:300), CXCL16 (dilution 1:360), CD68 (dilution 1:400), MPO (dilution 1:400), citrullinated histone H3 (CitH3) (dilution 1:400), CD11b (dilution 1:400),  $\alpha$ -SMA (dilution 1:400) were respectively incubated overnight at 4°C. After washing, the sections were incubated with goat anti-mouse IgG (H+L) highly cross-adsorbed 488 secondary antibody or anti-rabbit IgG (H+L) 594 secondary antibody (Thermo Fisher Scientific, Waltham, USA) and stained with DAPI. After staining of cell nuclear, the sections were sealed with resin and further observed using Aperio Versa (Leica, Wetzlar, Germany).

## 2.4 RNA-sequencing and bioinformatics analysis

The total RNA of liver from Mdr2<sup>-/-</sup> mice was extracted and then quantitated by NanoRhatometer<sup>®</sup>spectrophotometer (IMPLEN, USA). The RNA Nano Assay kit was used to measuring the integrity of RNA and the poly-T oligo-attached magnetic beads were applied for purifying the mRNA. After synthesizing the cDNA, the AMPure XP system (Beckman Coulter, USA) was used to purify the library fragments to enrich cDNA fragments in 250-300 bp. Furthermore, the sequencing library was established by the NEBNext Ultra<sup>TM</sup> RNA Library Prep Kit (NEB) and generated on the Illumina Novaseq platform as previously described (Li et al., 2022). Subsequently, sequencing samples were normalized and differentially expressed genes (DEGs) were analyzed using the edgeR software. Gene ontology (GO) enrichment analysis of DEGs was performed using the cluster Profiler R package. Gene set enrichment analysis

(GSEA) was used for in-depth analysis of the data, and hierarchical clustering analysis was performed using the heatmap R package. For GSEA analysis, we used DESeq2 as a ranking metric for conducting enrichment analysis of gene sets (<http://software.broadinstitute.org/gsea/index.jsp>). This method was used to determine whether target genes display statistically significant and consistent differences between two biological samples. For WGCNA analysis, according to these coding genes' expression profiles, the WGCNA co-expression algorithm was used to mine the co-expressing coding genes and co-expression modules. First, protein-encoding genes' expression profiles were extracted from the COAD expression profiles in the TCGA database, and the samples were clustered using hierarchical clustering. Outliers were removed and the rest samples were retained; further, the Pearson correlation coefficient was used to calculate the distance between each gene. The R software package WGCNA was used to construct a weighted co-expression network.

### 2.7 Cell isolation, culture, and treatment

RAW cells (macrophage cell line) and LX-2 cells (HSC cell line) were cultured in DMEM medium (10% FBS) and incubated at 37°C with 5% CO<sub>2</sub>. For the preparation of conditional medium, cellular RNA and protein, RAW cells were treated with LPS (50 ng/mL), IFN- $\gamma$  (2.5 ng/mL) and/or PIC II (5, 10, 20 mM) for 24 h and further collected for RNA or protein extraction. The medium derived from above macrophages was then collected for protein extraction and subsequently used as conditioned medium (conditional medium of macrophages, named as CM-M) for establishing the co-culture systems of HSCs, NK cells, and neutrophils subsequently. The primary NK cells were isolated from mouse spleen using the NK extraction kit (P9310) purchased from Solarbio science & technology Co., Ltd (Beijing, China). The cells were pseudo-suspension cultured for about 6 h (Fehniger et al., 1997; Sliz et al., 2019), and then treated with PBS or different groups of CM-Ms. The cells were collected after 24 h of culture for subsequent experiments. For the co-culture of NK cells and LX-2 cells, HSCs ( $1 \times 10^5$  cells per well of a 6-well plate) were pre-treated by the fibroblast inducible factor TGF- $\beta$  for 24 h, then the isolated NK cells ( $1 \times 10^6$  cells per well of a 6-well plate), which has been pre-activated by IL-2 or CM-M for 6 h, were added at a ratio of 10:1 to establish the co-culture system for 24 h (Melhem et al., 2006) (**Fig. 5A**). Then the cells and treat medium were collected for subsequent tests. The primary neutrophils were isolated from mouse bone marrow using a neutrophil extraction kit (P8550-200ml) purchased from Solarbio likewise. The cells were pseudo-suspension cultured for about 4 h, then treated with LPS (50 ng/mL) and/or PIC II (5, 10 and 20 mM). After treatment, cell samples were further collected for subsequent immunofluorescence experiments or RNA extraction. For the co-culture of neutrophils and HSCs, activated HSCs (pre-treated by TGF- $\beta$ ) were co-cultured with isolated neutrophils at a ratio of 1 : 3 with the presence of different dose of PIC II for 24 h (Casini et al., 1997; Zhou et al., 2018). After 24 h, cell samples were collected for extraction of cellular proteins, RNA or immunofluorescence analysis.

### 2.5 Transwell assay of NK cells and macrophages

After extraction and concentration, a total of  $1 \times 10^5$  NK cells were added in the top chamber of the transwell systems (0.4  $\mu$ m) with 1% FBS DMEM medium,  $1 \times 10^5$  attached macrophages were added in the lower chamber of the transwell systems with 1% FBS DMEM medium and treated with LPS (50 ng/mL), IFN- $\gamma$  (2.5 ng/mL), and different doses of PIC II (5, 10, 20 mM) for 6 h (**Fig. 4D**).

### 2.6 Flow cytometry analysis

Isolated primary NK cells were co-cultured with TGF- $\beta$ -treated HSCs at the ratio of 10:1 as previously described (Melhem et al., 2006). After attached, co-cultured cells were treated with CM of macrophages for 24 h and collected after digestion without EDTA and centrifuged at 2000 g for 5 minutes at 4°C. Fixed cells by paraformaldehyde were first incubated with  $\alpha$ -SMA antibody (1 : 400) and 5  $\mu$ l 7-AAD solution from 7-AAD staining kit (BD Biosciences, CA, USA). For  $\alpha$ -SMA staining, cells were stained with 4 $\mu$ M Goat anti-Rabbit IgG (H+L) Secondary Antibody Alexa Fluor 488 for 30 min in the dark at room temperature and further stained with 7-AAD binding buffer offered by staining kit. Then the  $\alpha$ -SMA/7-AAD signal were detected by the CytoFLEX flow cytometer (Beckman Coulter, Pasadena, CA), and the FlowJo software (v.10.3) was used for subsequent analysis of relative data.

## 2.7 Statistical analysis

All data were repeated at least three times and presented as mean  $\pm$  SD. Statistical analysis was conducted by one-way ANOVA analysis using GraphPad Prism version 8.0 program. Statistical significance was considered with a  $P$  value of [?] 0.05.

Additional method information and details were provided in the **Supplementary file** online.

## Results

### 3.1 PIC II significantly alleviates hepatic fibrosis and inflammation in *Mdr2*<sup>-/-</sup> mice

To broadly analyze the potential pharmacological effects of PIC II on hepatic fibrosis, we attempted to use the *Mdr2*<sup>-/-</sup> mice that mimics the immunopathogenesis and symptoms of patients with liver fibrosis in the clinic (**Fig. 1A**, left panel). As shown in **Fig. 1A**, right panel and **Fig. S1A**, there was little difference in the weight loss, ratio of liver or spleen to body weight between different groups. We further applied H & E and Masson's trichrome staining to evaluate the pathological change before or after PIC II administration and found that the obvious inflammatory infiltration, ECM deposition, and fibrous scar were observed in the liver of *Mdr2*<sup>-/-</sup> mice but were markedly alleviated by different doses of PIC II to varying degrees (**Fig. 1B**). Consistently, although it had less effects on  $\gamma$ -glutamyl transpeptidase ( $\gamma$ -GGT) (a cell surface enzyme for indicating hepatobiliary injury, **Fig. S1B**), PIC II at different concentrations also significantly downregulated the serum levels of aspartate aminotransferase (AST) and alanine aminotransferase (ALT, two typical markers for hepatic injury), total biliary acid (TBA), total bilirubin (TBIL) and alkaline phosphatase (AKP, three markers for reflecting bile acid accumulation and liver fibrosis degree) induced by the deficiency of *Mdr2* (**Fig. 1C** and **Fig. S1B**). To better figure out the protective effects and underlying mechanisms of PIC II, we further performed RNA-sequencing analysis of fibrotic livers in *Mdr2*<sup>-/-</sup> mice and plotted DEGs implicated in fibrosis-related genes as a heatmap (**Fig. 1D**). A total of 8274 DEGs with  $P$ -value  $<$  0.05 was identified between three different groups. In cluster 1, the expression of genes was downregulated in the *Mdr2*<sup>-/-</sup> mice and further decreased in *Mdr2*<sup>-/-</sup> + PIC II group, such as *Stat3*, ribosomal protein S6 (*Rps6*) and small mother against decapentaplegic family member 3 (*Smad3*), which often early increased and sustained in liver injury. The gene expression in cluster 2 was upregulated in the *Mdr2*<sup>-/-</sup> group and further increased in *Mdr2*<sup>-/-</sup> + PIC II group, such as the key genes involved in inhibiting HSC proliferation and activation like peroxisome proliferator activated receptor gamma (*Pparg*) and *Smad7* as well as collagen degradation related gene including matrix metalloproteinase 13 (*Mmp13*). The expression of DEGs in cluster 3 including cellular communication network factor 2 (*Cnn2*) as well as collagen formation genes such as tissue inhibitor of metalloproteinase 1 (*Timp1*) and collagen type XXIII alpha 1 chain (*Col23a1*) in cluster 4 were remarkably downregulated in the *Mdr2*<sup>-/-</sup> + PIC II group when compared to the *Mdr2*<sup>-/-</sup> group (**Fig. 1D**). Consistently, the qPCR results validated the mRNA changes of representative fibrosis-related genes in the heatmap and showed that PIC II mainly inhibited the expression of the collagen-synthesis related genes (*Fn1*, *Acta2*, *H19* and *Colla1*) and positively supported the collagen-degradation related ways (increased *Mmp13* and *Timp1*) (**Fig. 1E**). Furthermore, the immunofluorescence staining also confirmed the anti-fibrotic effects of PIC II on the *Mdr2*<sup>-/-</sup> mouse model, as illustrated by the lower distribution of Fibronectin,  $\alpha$ -SMA and Collagen1 (**Fig. 1F** and **Fig. S1C**). Of noted, the direct inhibition of PIC II on the protein level of  $\alpha$ -SMA and fibronectin in aHSC had not been observed clearly (**Fig. S2A** and **S2B**), which suggested that PIC II might possess a suppressive effect on aHSCs through another indirect way.

### 3.2 PIC II may attenuate hepatic fibrosis via improving hepatic immune microenvironment in *Mdr2*<sup>-/-</sup> mice

In order to investigate whether the anti-fibrotic effects of PIC II were relied on the regulation of different immune cells, we systematically analyzed the RNA-sequencing data and try to figure out the primary target genes that PIC II might focus on. Based on the different modules of gene expression of all DEGs, WGCNA was used to construct a gene co-expression network with the *Pearson's* correlation coefficient applying to cluster the sample, and simultaneously, eight modules were then obtained through the hierarchical clustering of the predetermined dissimilarities in **Fig. 2A**. To pick out the liver fibrosis-related modules, the relationship between the modules and the result of hepatic pathology and function was studied. Among the 8 modules,

the turquoise and blue module was highly associated with pathological manifestation, thus they were selected for further analysis. Additionally, three co-expression modules, including inflammatory infiltration, collagen deposition and oxidative stress were mainly enriched, especially for inflammatory infiltration governing the liver fibrosis (**Fig. 2B**). Therefore, we speculate that PIC II might exert a potential effect through immune cells and thus we plotted DEGs implicated in immune-related targets as a heatmap and prepared relative clusters (**Fig. 2C**). Compared with the WT group, it was found that most differential genes were enriched in cluster 3, which were upregulated in model and PIC II mice, including the macrophage makers *Cd86*, colony stimulating factor 2 receptor subunit alpha (*Csf2ra*) and *Csf3r*, and NK cell activation cytokines like C-C motif chemokine ligand 3 (*Ccl3*) and interleukin 4 receptor, alpha (*Il4ra*). After noticing the significant changes in immune reactions, different subtypes of immune cells in three different groups were analyzed, we then investigated that PIC II could remarkably affect the proportion of macrophages (**Fig. 2D**). Generally, M1 macrophages were known as a stimulator of inflammatory reaction while M2 macrophage more likely contributes to the remission of liver fibrosis (Cheng et al., 2021). Notably, a further grouping of quantitative differences exhibited that PIC II increased the numbers of M1 macrophages and monocytes but didn't decrease the number of M2-type macrophages and NK cells, compared with *Mdr2<sup>-/-</sup>* mice (**Fig. 2E** and **2F**). These results indicated that PIC II might alleviate fibrosis through establishing intricate links among diversified immune cells, which was far more complex than we traditionally imaged.

### 3.3 PIC II enhances the function of M1-polarized macrophages and promotes the release of chemokine CXCL16

Recently, M1-polarized macrophages were proved to ameliorate the liver fibrosis through modulating immune microenvironment in the carbon tetrachloride (CCl<sub>4</sub>)- and bile duct ligation (BDL)-induced liver fibrosis mice (Ma et al., 2017). Hence, we investigated whether and how PIC II regulated the genes involved in the function and polarization of macrophages. According to the heatmap shown in **Fig. 3A**, DEGs enriched in the macrophages-related inflammatory factors and M1-polarized macrophages-related pathways were significantly changed in the *Mdr2<sup>-/-</sup>* + PIC II group, compared with the *Mdr2<sup>-/-</sup>* group. In cluster 1, the expression of genes was upregulated in the *Mdr2<sup>-/-</sup>* group and was further decreased in *Mdr2<sup>-/-</sup>* + PIC II group, such as the spondin 2 (*spon2*) and *ccl5*, and other cell adhesion-related genes. Of note, the expression of genes in cluster 3 mainly associated with M1-polarized macrophage was upregulated in the *Mdr2<sup>-/-</sup>* + PIC II group, especially genes related to the chemotactic ability of activated M1 macrophages (including *Cd80*, *Cxcl16* and nitric oxide synthase 2 [*Inos*]). Interestingly, *cd163* in cluster 4 indicated the expansion of phagocytosis accompanying with increased macrophage activity. The consistent GSEA plot results also demonstrated that DEGs enriched in M1-polarized macrophages maker genes were significantly upregulated in the *Mdr2<sup>-/-</sup>* + PIC II group when compared to the *Mdr2<sup>-/-</sup>* group (**Fig. 3B**). Subsequently, our qPCR results in **Fig. 3C** showed that the macrophages in the fibrotic liver of mice appeared not to be polarized into inflammatory state, because PIC II did not up-regulate inflammatory markers including *il6* and *inos*, slightly increase *Cd163* and decrease the M2-type macrophage maker transglutaminase 2 (*Tgm2*). Meanwhile, the expressions of *Mmp13* and *Mmp2* were significantly upregulated after PIC II treatment, consistent with the downregulated *Fn1* (**Fig. 3D**). Interestingly, among those different subsets of changed chemokines listed in **Fig. 3A**, *Cxcl16*, *Cxcl1*, *Cxcr2* and *Ccl5* were detected by qPCR and *cxcl16* showed the clear upregulation in the *Mdr2<sup>-/-</sup>* + PIC II group when compared with the WT group in **Fig. 3D** and **Fig. S3A**. Consistently, PIC II markedly enhanced the hepatic expression and intrahepatic distribution of CXCL16 in the liver of *Mdr2<sup>-/-</sup>* mice (**Fig. 3E**, **3F** and **Fig. S3B**). We also confirmed that PIC II at different dosages dramatically increased the hepatic level of chemokine CXCL16 in M1-type macrophages induced by the administration of IFN- $\gamma$  and LPS and promoted its secretion into culture medium (CM) (**Fig. 3G-3I** and **Fig. S3C**). Taken together, these results suggested that PIC II promoted the M1-polarized macrophages and further triggered the production and secretion of CXCL16 from these macrophages of *Mdr2<sup>-/-</sup>* mice. Meanwhile, since the CM of CXCL16 highly expressed M1 macrophages didn't show a significant inhibitory effect on the HSC activation (**Fig. S3D**), we then transfer our attention to find another way to figure out how the M1 macrophages affect the liver fibrosis process.

### 3.4 PIC II promotes CXCL16-expressed M1 macrophages to recruit and activate NK cells

Although PIC II was not found to have visibly impact on the dominant amount of NK cells before (**Fig. 2E**), the heatmap results in **Fig. 4A** still exhibited that DEGs enriched in the inflammatory cytokines especially for the markers of NK cells, including *Ifngr*, neural cell adhesion molecule 1 (*Ncam1*), integrin subunit alpha 1 (*Itga1*) and NK cell-mediated target cell killing pathways such as *Gzmb* were changed after PIC II administration. Similar results of GSEA plots further confirmed that the DEGs enriched in NK cells-mediated immune response were significantly downregulated in the *Mdr2*<sup>-/-</sup> group but were increased by PIC II administration (**Fig. 4B**). Simultaneously, we validated the protein expression of NK cell-mediated cell killing-related targets and proved that PIC II slightly increased or maintained the expressions of PERFORIN and GZMB, more importantly, markedly increased the expression of C-X-C motif chemokine receptor 6 (CXCR6, the surface receptor of NK cells) and the apoptosis-inducing factor STAT1 in the *Mdr2*<sup>-/-</sup> mice (**Fig. 4C** and **Fig. S4A**). Considering the recruitable feature of NK cells and the characteristic of interaction between immune cells in liver fibrosis, we next construct a co-culture system of macrophages and NK cells to explore whether and how M1 polarized macrophage regulated the activity of NK cells in the *Mdr2*<sup>-/-</sup> mice. In brief, we seeded M1-type macrophages induced by IFN plus LPS in the lower cell plate and further plated primary NK cells in the upper transwells (**Fig. 4D**). As expected, transwell migration assay also demonstrated that after being treated with PIC II, CM secreted by M1-type macrophages (namely CM-M) in different groups promoted the recruitment of NK cells (**Fig. 4E**). Likewise, the immunofluorescences co-staining of CD161 (NK1.1) and CXCL16 confirmed that PIC II at different dosages increased the expression of CXCL16 in co-cultured NK cells (**Fig. 4F** and **Fig. S4B**), even without significant upregulation of cytotoxicity factors of PERFORIN and GZMB. Previous studies have demonstrated the multiple roles of CXCR6 on HSC activation, fibrogenesis, and proliferation, and the activation of NK might lead to HSCs apoptosis (Ma et al., 2017). Therefore, we further detected whether CXCL16 released from PIC II-treated macrophages may recognized by CXCR6 expressed on NK cells. The relative mRNA levels of *Cxcr6* both in *in vivo* and *in vitro* were increased after PIC II administration in livers of *Mdr2*<sup>-/-</sup> mice and co-cultured NK cells (**Fig. 4G** and **4H**). These results suggested that PIC II promoted M1-polarized macrophages to recruit and activate NK cells by the CXCL16-CXCR6 pathway.

### 3.5 PIC II facilitated NK cells to kill activated HSCs dependent on IFN- $\gamma$ -*Jak1/Tyk2*-*STAT1* pathway

To further elucidate whether NK cells activated by macrophages could kill aHSCs, we then isolated primary NK cells from the spleen of mice, which were pre-treated with IL-2 and/or CM-M with different doses of PIC II and were then co-cultured with activated HSCs induced by TGF- $\beta$  in a 10 : 1 ratio (**Fig. 5A**). The purity of NK cells (CD16, CD56, and the staining of CD161 marked the activity of NK cells) isolated from mice have been tested (**Fig. S5A** and **S5B**). As shown in **Fig. 5B**, the cell viability of co-culture cells in the model group and PIC II CM-treated group were all significantly decreased. Additionally, we examined the mRNA levels of fibrosis-related targets in co-culture cells and found that with the presence of PIC II-treated NK cells, the expression of *Acta2*, *Col1a1* and *Fn1* (fibrotic markers mainly expressed in HSCs) were markedly decreased (**Fig. 5C**). This result was further refined by flow cytometry analysis stained with both  $\alpha$ -SMA antibody and 7-AAD of co-culture cells to distinguish two different types of cells. As shown in **Fig. 5D**, compared to the model group, PIC II increased the HSC death that marked by both  $\alpha$ -SMA and 7-AAD in a dose-dependent manner, according to the clearly separated cell clusters. Meanwhile, immunofluorescence staining results showed that CM-M containing different doses of PIC II significantly reduced the expression of  $\alpha$ -SMA in co-culture of HSC-NK cells (**Fig. 5E**). After we preliminarily confirm that activation and viability of HSCs could be inhibited by NK cells recruited by M1 macrophages, we intended to further explore the underlying mechanisms among these immune cells and HSCs.

Notably, NK cells can suppress aHSC populations *via* directly killing activated or senescent HSCs. However, the directly cytotoxicity of PERFORIN and GZMB released by NK cells on HSCs have been not upregulated significantly as expected (**Fig. S6** and **S4A**). On the other hand, the inhibitive effects of NK cells on HSCs are also relied on the IFN- $\gamma$ -related network. Interestingly, we noticed an obvious upregulation of *Ifng* after administration of PIC II both in *Mdr2*<sup>-/-</sup> mouse livers (**Fig. 6A**) and in co-culture system of HSC and NK cells (**Fig. 6B**). Indeed, the interaction of IFN- $\gamma$  and its receptor at the cell surface was reported to lead the activation of JAK1 and TYK2, resulting in the phosphorylation and nuclear translocation of STAT1

and directly lead to the transcription of genes involved in cell apoptosis (Martí-Rodrigo et al., 2020). As shown in **Fig. 6C**, compared with the *Mdr2*<sup>-/-</sup> mice, we found that the phosphorylation of Jak1, Tyk2 and its downstream factor STAT1 were all upregulated in the mouse liver after treated with different doses of PIC II. Notably, phosphorylated STAT1 was mainly translocated in the nucleus after PIC II administration, which suggested that NK cells processing an inhibited effect on aHSC mainly mediated by the release of IFN- $\gamma$ . We also verified the hypothesis through the co-culture system as previously shown in **Fig. 5A**. Consistently, we noticed that the *Ifng* level in NK cells was upregulated by PIC II (**Fig. 6B**), followed by the phosphorylation of Jak1 and Tyk2 and both the phosphorylation and nuclear translocation of STAT1 in the co-cultured HSCs and NK cells (**Fig. 6D**). These results suggested that after recruited by M1-macrophages released CXCL16, PIC II might facilitate NK cells to kill aHSCs dependent on IFN- $\gamma$ -Jak1/Tyk2-STAT1 pathway.

### 3.7 PIC II inhibited the neutrophil extracellular traps (NETs) formation and promoted the rupture of aHSCs

Considering the virtual role of intercellular communication between immune cells and HSCs played in the liver fibrosis, we further investigated whether PIC II influenced neutrophils, another type of crucial cell existed in the hepatic immune microenvironment. First, we conducted GSEA plots and revealed that DEGs associated with neutrophil inhibition was significantly increased in the *Mdr2*<sup>-/-</sup> + PIC II group when compared to the *Mdr2*<sup>-/-</sup> group (**Fig. 7A**). Based on RNA sequencing results, the expression of DEGs, enriched in integrins and cytokines, were presented as a heatmap with 4 clusters by hierarchical cluster analysis. As shown in **Fig. 7B**, PIC II markedly decreased the level of neutrophil chemotaxis markers (*Cxcl1*, *Cxcl2*) and notably, increased the level of neutrophil senescence marker *Cxcr4* and decreased the level of neutrophil makers (lymphocyte antigen 6 complex, locus G [*Ly6g*], *Ly6g5b* and *Ly6g6d*). These results suggested that PIC II might not only recruited NK cells via releasing CXCL16 and combining with CXCR6 but also accelerate the senescence of neutrophils at the same time, which broadens the possibility of interrelations taken place among these distinct immune cells in the liver fibrosis process.

The other remarkable thing is that neutrophil-derived fibrous networks, NETs, often lead a worsen immune and microvascular circumstances resulting in anabatic hepatic liver fibrosis. Therefore, we performed immunofluorescence staining of NETs markers CitH3 and MPO and found that PIC II markedly reduced the formation of extracellular NETs in *Mdr2*<sup>-/-</sup> mice (**Fig. 7C** and **Fig.S7**). Similarly, the serum level of MPO (**Fig. 7D**) and relative mRNA levels of genes associated with neutrophils, such as the *Ly6g*, were dramatically increased in the *Mdr2*<sup>-/-</sup> group. Interestingly, although PIC II didn't affect the expression of *Ly6g*, it markedly decreased MPO level, and intercellular adhesion molecule 1 (*Icam1*) mRNA expression, and increased the senescence maker of neutrophils (*Cxcr4*) in the fibrotic liver (**Fig. 7E**). In consideration of the inflammatory crosstalk between neutrophils and HSCs in hepatic fibrosis, we further explored the effects of PIC II on primary activated neutrophils and co-cultured system of neutrophils and HSCs. Consistently, PIC II markedly reduced the formation of NETs induced by IL-2, a classical activator of neutrophils (**Fig. 7F**) and dose-dependently promoted the rupture of activated HSCs with the presence of CM from PIC II-treated NK cells (namely CM-Neu) (**Fig. 7G**), suggesting the inhibitory effects of PIC II on aHSCs might be also attributed to the restriction of neutrophil activation and NETs formation.

### 3.8 The depletion of macrophage partially neutralizes the anti-fibrotic effect of PIC II

Based on the vital role of macrophages played in the fibrotic liver of *Mdr2*<sup>-/-</sup> mice, we then verified that whether the depletion of macrophages will obstruct PIC II-induced hepatoprotective effects in a negative manner. The clodronate liposome (CL), a classical scavenger agent targeting on macrophages, was used for macrophage depletion in *Mdr2*<sup>-/-</sup> mice treated with or without PIC II (**Fig. 8A**). Compared with the *Mdr2*<sup>-/-</sup> group, CL markedly increased the levels of TBA, TBIL, AST, ALT, and  $\gamma$ -GGT in serum, which was almost unchanged or only slightly decreased in *Mdr2*<sup>-/-</sup> + CL + PIC II group in **Fig. 8B** and **Fig. S8A**. We further evaluated the pathological change after macrophage clearance and observed similar changes of inflammatory infiltration, ECM deposition, and fibrous scar in the *Mdr2*<sup>-/-</sup> + macrophage depletion group and *Mdr2*<sup>-/-</sup> + CL + PIC II group (**Fig. 8C**). Meanwhile, CXCL16 was proved to decreased and not to co-located with F4/80 both in the *Mdr2*<sup>-/-</sup> + CL group and *Mdr2*<sup>-/-</sup> + CL + PIC II group (**Fig. 8D**). To

better evaluate the protective effects and underlying mechanisms of PICII after macrophage clearance, we also performed qPCR to detect the gene expression of interest. Although the mRNA levels of *Cxcl16* was similar before or after CL treatment, the typical marker of M1 polarized macrophages, *Inos*, was down-regulated both in the *Mdr2*<sup>-/-</sup> + CL group and *Mdr2*<sup>-/-</sup> + CL + PIC II group. Besides, the meaningful changes of other immune cells were also checked as following: the phagosome marker *Rab7a* has not been changed evidently, the cytotoxic maker of NK cells *Il4* was found to slightly decreased, and the neutrophils marker *Ly6g* was noticed to up-regulated in *Mdr2*<sup>-/-</sup> + CL group while being down-regulated in *Mdr2*<sup>-/-</sup> + CL + PIC II group, which might evidence that PIC II showed an inhibitory effect on neutrophils in liver fibrotic process. Interestingly, along with the changes of immune cells makers, the fibrotic gene expression like *Fn1* and *Col1a1* and *Acta2* remains high and PIC II could not decrease their expression once macrophage depletion in *Mdr2*<sup>-/-</sup> mice (**Fig. 8E** and **Fig. S8B**). Meanwhile, the protein levels of FIBRONECTIN and COLLAGEN in **Fig. 8F** also showed the similar trend in above relative groups. These results suggest that depletion of macrophages at least partially neutralized PIC II-induced hepatoprotective effects in *Mdr2*<sup>-/-</sup> mice.

#### 4. Discussion

Liver fibrosis is a global epidemic, characterized by the activated myofibroblasts through secreting ECM proteins and chronic interminable inflammation initiated and exaggerated by macrophages, dendritic cells, NK cells, and neutrophils. In the complex hepatic immune network, macrophages generally initiate adaptive immune inflammatory responses and release or stimulate paracellular cells to release various cytokines, which profoundly affect the activation, senescence, or apoptosis of HSCs (Kisseleva & Brenner, 2021; Tacke & Zimmermann, 2014). In this study, we explored the anti-fibrotic effect of PIC II on the liver fibrosis in *Mdr2*<sup>-/-</sup> mice and found that PIC II might inhibit the activation of HSCs *via* affecting various immune cells. Specifically, the increase of M1-polarized macrophages was observed in livers of *Mdr2*<sup>-/-</sup> mice treated with PIC II, accompanied with highly expressed CXCL16 and obviously decreased fibrotic markers (**Fig. 1** and **2**). Although PIC II exerted a slightly inhibitory effect on aHSCs, it significantly promotes the function of M1 polarized macrophages without inducing inflammation and facilitates the release of CXCL16 into the extracellular environment (**Fig. 3**). Next, we noticed the changes of NK cells in *Mdr2*<sup>-/-</sup> mice and found that NK cells were recruited by CXCL16 released from PIC II-treated M1-type macrophages depend on the CXCR6 expressed on its cellular surface (**Fig. 4**). Furthermore, under the stimulation of PIC II, the IFN- $\gamma$  secreted by NK cells activated and phosphorylated the JAK1/TYK2 to promote the nuclear translocation of STAT1 and eventually induce cell death of activated HSCs (**Fig. 6**). In addition, PIC II processing an inhibitive effect on neutrophils through blocking the NETs formation and possibly inducing the senescence of neutrophils for eventually preventing the more severe activations of HSCs in fibrotic environment (**Fig. 7**), and the depletion of macrophage will largely counteract this kind of protective effects of PIC II (**Fig. 8**).

As the central immune cells in liver fibrosis procedure, macrophages play an important role in both regulating the deposition and breakdown of ECM. Emerging studies have shown that distinct macrophage subsets exert bidirectional roles and contribute to different pathological outcomes of liver fibrosis (Rao et al., 2022; Tacke, 2017). Activated macrophages have reportedly release various cytokines like NF- $\kappa$ B, TGF- $\beta$  and activated TLRs to aggravate liver fibrosis by increasing the survival of activated HSCs (Rao et al., 2022). Whereas, M1 macrophages are recently treated as cryotherapy targets, which possess anti-liver fibrosis effects by recruiting endogenous macrophages and NK cells to inhibit HSC proliferation through MMPs (MMP2, MMP9, MMP13), IFN- $\gamma$  and TRAIL (Ma et al., 2017). Our sequencing data showed that PIC II markedly increased M1-polarized macrophages and promoted the secretion of several cytokines such as CXCL16 under the fibrotic environment, but exerting a limited direct inhibitory effect on aHSCs (**Fig. 2** and **3**). Considering the gene expression of *IFN- $\gamma$* , *Itga1* and *Gzmb*, and the recruited characteristic of NK cells, we supposed that the CXCL16-positive M1 macrophage may recruit the NK cells and inhibit liver fibrosis in *Mdr2*<sup>-/-</sup> mice through CXCR6 that expressed on the surface of NK cells in concert with CXCL16.

The increase in both quantity and activity of NK cells has been acknowledged to provide a salutary effect in alleviating the progression of liver fibrosis (Tsuchida & Friedman, 2017). On one hand, NK cells recruited

by macrophages can directly promote HSC apoptosis and ultimately hinder the fibrogenesis through the upregulation of GZMB and PERFORIN (Chigbu et al., 2019; Choi et al., 2021). On the other hand, NK cells can also interfere with the activation pathway of HSCs *via* activating IFN- $\gamma$ -JAK1/TYK2-STAT1 signaling. Usually, IFN- $\gamma$  was recognized to binds to its receptors IFNGR1 and IFNGR2 (Guo et al., 2022; Wen et al., 2017), then promote the phosphorylation of JAKs, TYK2 and STAT1. Indeed, JAKs/STATs pathway plays key roles in controlling chronic liver injury progression and liver regeneration. Also, among these STATs, the activation of STAT1 promotes the apoptotic signal in HSCs and eventually limits the development of liver fibrosis. Recently, Alberto and his colleague demonstrated that rilpivirine could ameliorate liver fibrosis by selectively activating the STAT1-dependent apoptosis in HSCs and STAT3-dependent regeneration in hepatocytes to promote liver reconstruction (Martí-Rodrigo et al., 2020). Likewise, our study reveals that after treated with PIC II, NK cells were recruited by CXCL16 released from M1 macrophages, activated to induce HSC apoptosis through the activation of JAK1/TAK2-STAT1 following the release of IFN- $\gamma$ , rather than directly killing HSCs by cytotoxic secretion of Gzmb and perforin (**Fig. 5** and **6**). These results offered a perspective to understand the interaction between the NK cells recruited by macrophages and HSCs in the liver fibrosis.

Interestingly, we also found a trend of neutrophil gene set and NETs formation in *Mdr2*<sup>-/-</sup> mouse livers. Previously, NETosis has been more commonly observed in NASH, liver cirrhosis/necrosis, and hepatocellular carcinoma (Scozzi & Gelman, 2023; Wu et al., 2023), but the MPO-citH3 index and the NETs formation results of liver tissue supported the hypothesis that NETs formation also occurs in the fibrotic and inflammatory environment of *Mdr2*<sup>-/-</sup> mouse livers. Here, we found the clear relevance between NETs formation and HSCs activation in *Mdr2*<sup>-/-</sup> mice and PIC II administration could not only inhibited the NETosis but also lessen the collagen formation during this fibrotic process. Interestingly, CXCR4 was often treated as a marker of aged neutrophils, which is a receptor allowing the clearance of neutrophils in the bone marrow (Zhang et al., 2015). Our results also showed that *Cxcr4* was upregulated in neutrophils recruited and downregulated in the PIC II administration group, which offered a possibility of neutrophils senescence and provided a potential mechanism that PIC II works in the liver fibrotic environment. However, the role and pattern of NETs under the crosstalk between M1 macrophages and neutrophils in this study are still uncertain, and further exploration is warranted.

It is also noteworthy that macrophages, as candidates for the treatment of liver fibrosis, have different polarization states and a wide range of plasticity spectra. Currently, the selective macrophage depletion could reduce BDL-induced fibrotic liver injury, which was accompanied by inhibition of lncRNA H19, while the overexpression of H19 could counteract the effects of macrophage depletion in liver fibrosis. (Tian et al., 2021). On the other hand, one fact that cannot be ignored is that CL could not selectively clear a specific subtype of macrophages in liver. Thus, there is another study reported that the depletion of macrophages *via* CL had no therapeutic effect on bile duct expansion in livers of *Anks6*<sup>-/-</sup> mice (Airik et al., 2022). In our study, the depletion of macrophage through CL effectively influenced the release of CXCL16 and partially blocked the anti-hepatic fibrosis effects of PIC II on the livers of *Mdr2*<sup>-/-</sup> mice (**Fig. 8**). Therefore, a single method of CL depletion may lead to complex and contradictory consequences due to different functions of hepatic macrophages and whether this method can be used for the treatment of liver fibrosis remains to be determined.

## 5. Conclusion

Collectively, we pointed out the importance of M1 macrophage-centered mutual interaction among immune cells in the fibrotic livers of *Mdr2*<sup>-/-</sup> mice and indicated that, through this rationale, PIC II is a potential candidate for halting the progression of liver fibrosis.

**Conflicts of interest:** The authors report no conflicts of interest. The authors alone are responsible for the content and writing of this article.

## References

Airik, M., McCourt, B., Ozturk, T. T., Huynh, A. B., Zhang, X., Tometich, J. T., . . . Airik, R. (2022).

- Mitigation of portal fibrosis and cholestatic liver disease in ANKS6-deficient livers by macrophage depletion. *Faseb j* , 36 (2), e22157.<https://doi.org/10.1096/fj.202101387R>
- Casini, A., Ceni, E., Salzano, R., Biondi, P., Parola, M., Galli, A., . . . Surrenti, C. (1997). Neutrophil-derived superoxide anion induces lipid peroxidation and stimulates collagen synthesis in human hepatic stellate cells: role of nitric oxide. *Hepatology* , 25 (2), 361-367.<https://doi.org/10.1053/jhep.1997.v25.pm0009021948>
- Cheng, D., Chai, J., Wang, H., Fu, L., Peng, S., & Ni, X. (2021). Hepatic macrophages: Key players in the development and progression of liver fibrosis. *Liver Int* , 41 (10), 2279-2294.<https://doi.org/10.1111/liv.14940>
- Chigbu, D. I., Loonawat, R., Sehgal, M., Patel, D., & Jain, P. (2019). Hepatitis C Virus Infection: Host-Virus Interaction and Mechanisms of Viral Persistence. *Cells* , 8 (4).<https://doi.org/10.3390/cells8040376>
- Choi, W. M., Ryu, T., Lee, J. H., Shim, Y. R., Kim, M. H., Kim, H. H., . . . Jeong, W. I. (2021). Metabotropic Glutamate Receptor 5 in Natural Killer Cells Attenuates Liver Fibrosis by Exerting Cytotoxicity to Activated Stellate Cells. *Hepatology* , 74 (4), 2170-2185.<https://doi.org/10.1002/hep.31875>
- Duan, S., Li, X., Fan, G., & Liu, R. (2022). Targeting bile acid signaling for the treatment of liver diseases: From bench to bed. *Biomed Pharmacother* , 152 , 113154.<https://doi.org/10.1016/j.biopha.2022.113154>
- Fehniger, T. A., Carson, W. E., Mrózek, E., & Caligiuri, M. A. (1997). Stem cell factor enhances interleukin-2-mediated expansion of murine natural killer cells in vivo. *Blood* , 90 (9), 3647-3653.
- Guicciardi, M. E., Trussoni, C. E., Krishnan, A., Bronk, S. F., Lorenzo Pisarello, M. J., O'Hara, S. P., . . . Gores, G. J. (2018). Macrophages contribute to the pathogenesis of sclerosing cholangitis in mice. *J Hepatol* , 69 (3), 676-686.<https://doi.org/10.1016/j.jhep.2018.05.018>
- Guo, M., Wang, Z., Dai, J., Fan, H., Yuan, N., Gao, L., . . . Cheng, X. (2022). Glycyrrhizic acid alleviates liver fibrosis in vitro and in vivo via activating CUGBP1-mediated IFN- $\gamma$ /STAT1/Smad7 pathway. *Phytomedicine* , 112 , 154587.<https://doi.org/10.1016/j.phymed.2022.154587>
- Huang, Y., Zhou, M., Li, C., Chen, Y., Fang, W., Xu, G., & Shi, X. (2016). Picoside II protects against sepsis via suppressing inflammation in mice. *Am J Transl Res* , 8 (12), 5519-5531.
- Kisseleva, T., & Brenner, D. (2021). Molecular and cellular mechanisms of liver fibrosis and its regression. *Nat Rev Gastroenterol Hepatol* , 18 (3), 151-166.<https://doi.org/10.1038/s41575-020-00372-7>
- Li, T., Xu, L., Zheng, R., Wang, X., Li, L., Ji, H., & Hu, Q. (2020). Picoside II protects against cholestatic liver injury possibly through activation of farnesoid X receptor. *Phytomedicine* , 68 , 153153.<https://doi.org/10.1016/j.phymed.2019.153153>
- Li, Y. J., Liu, R. P., Ding, M. N., Zheng, Q., Wu, J. Z., Xue, X. Y., . . . Li, X. (2022). Tetramethylpyrazine prevents liver fibrotic injury in mice by targeting hepatocyte-derived and mitochondrial DNA-enriched extracellular vesicles. *Acta Pharmacol Sin* , 43 (8), 2026-2041.<https://doi.org/10.1038/s41401-021-00843-w>
- Liu, R., Li, X., Zhu, W., Wang, Y., Zhao, D., Wang, X., . . . Zhou, H. (2019). Cholangiocyte-Derived Exosomal Long Noncoding RNA H19 Promotes Hepatic Stellate Cell Activation and Cholestatic Liver Fibrosis. *Hepatology* , 70 (4), 1317-1335.<https://doi.org/10.1002/hep.30662>
- Liu, Y., Chen, K., Li, F., Gu, Z., Liu, Q., He, L., . . . Feng, W. (2020). Probiotic *Lactobacillus rhamnosus* GG Prevents Liver Fibrosis Through Inhibiting Hepatic Bile Acid Synthesis and Enhancing Bile Acid Excretion in Mice. *Hepatology* , 71 (6), 2050-2066.<https://doi.org/10.1002/hep.30975>
- Ma, P. F., Gao, C. C., Yi, J., Zhao, J. L., Liang, S. Q., Zhao, Y., . . . Qin, H. Y. (2017). Cytotherapy with M1-polarized macrophages ameliorates liver fibrosis by modulating immune microenvironment in mice. *J Hepatol* , 67 (4), 770-779.<https://doi.org/10.1016/j.jhep.2017.05.022>

- Ma, S., Wang, X., Lai, F., & Lou, C. (2020). The beneficial pharmacological effects and potential mechanisms of picoside II: Evidence of its benefits from in vitro and in vivo. *Biomed Pharmacother* , 130 , 110421. <https://doi.org/10.1016/j.biopha.2020.110421>
- Martí-Rodrigo, A., Alegre, F., Moragrega Á, B., García-García, F., Martí-Rodrigo, P., Fernández-Iglesias, A., . . . Blas-García, A. (2020). Rilpivirine attenuates liver fibrosis through selective STAT1-mediated apoptosis in hepatic stellate cells. *Gut* , 69 (5), 920-932. <https://doi.org/10.1136/gutjnl-2019-318372>
- Melhem, A., Muhanna, N., Bishara, A., Alvarez, C. E., Ilan, Y., Bishara, T., . . . Safadi, R. (2006). Anti-fibrotic activity of NK cells in experimental liver injury through killing of activated HSC. *J Hepatol* , 45 (1), 60-71. <https://doi.org/10.1016/j.jhep.2005.12.025>
- Parola, M., & Pinzani, M. (2019). Liver fibrosis: Pathophysiology, pathogenetic targets and clinical issues. *Mol Aspects Med* , 65 , 37-55. <https://doi.org/10.1016/j.mam.2018.09.002>
- Rao, J., Wang, H., Ni, M., Wang, Z., Wang, Z., Wei, S., . . . Lu, L. (2022). FSTL1 promotes liver fibrosis by reprogramming macrophage function through modulating the intracellular function of PKM2. *Gut* , 71 (12), 2539-2550. <https://doi.org/10.1136/gutjnl-2021-325150>
- Ravichandran, G., Neumann, K., Berkhout, L. K., Weidemann, S., Langeneckert, A. E., Schwinge, D., . . . Tieg, G. (2019). Interferon- $\gamma$ -dependent immune responses contribute to the pathogenesis of sclerosing cholangitis in mice. *J Hepatol* , 71 (4), 773-782. <https://doi.org/10.1016/j.jhep.2019.05.023>
- Scozzi, D., & Gelman, A. E. (2023). Avoid being trapped by your liver: ischemia-reperfusion injury in liver transplant triggers S1P-mediated NETosis. *J Clin Invest* , 133 (3). <https://doi.org/10.1172/jci167012>
- Shah, R. A., & Kowdley, K. V. (2020). Current and potential treatments for primary biliary cholangitis. *Lancet Gastroenterol Hepatol* , 5 (3), 306-315. [https://doi.org/10.1016/s2468-1253\(19\)30343-7](https://doi.org/10.1016/s2468-1253(19)30343-7)
- Shi, T., Malik, A., Yang Vom Hofe, A., Matuschek, L., Mullen, M., Lages, C. S., . . . Miethke, A. G. (2022). Farnesoid X receptor antagonizes macrophage-dependent licensing of effector T lymphocytes and progression of sclerosing cholangitis. *Sci Transl Med* , 14 (675), eabi4354. <https://doi.org/10.1126/scitranslmed.abi4354>
- Sliz, A., Locker, K. C. S., Lampe, K., Godarova, A., Plas, D. R., Janssen, E. M., . . . Hoebe, K. (2019). Gab3 is required for IL-2- and IL-15-induced NK cell expansion and limits trophoblast invasion during pregnancy. *Sci Immunol* , 4 (38). <https://doi.org/10.1126/sciimmunol.aav3866>
- Tacke, F. (2017). Targeting hepatic macrophages to treat liver diseases. *J Hepatol* , 66 (6), 1300-1312. <https://doi.org/10.1016/j.jhep.2017.02.026>
- Tacke, F., & Zimmermann, H. W. (2014). Macrophage heterogeneity in liver injury and fibrosis. *J Hepatol* , 60 (5), 1090-1096. <https://doi.org/10.1016/j.jhep.2013.12.025>
- Taylor, A. E., Carey, A. N., Kudira, R., Lages, C. S., Shi, T., Lam, S., . . . Miethke, A. G. (2018). Interleukin 2 Promotes Hepatic Regulatory T Cell Responses and Protects From Biliary Fibrosis in Murine Sclerosing Cholangitis. *Hepatology* , 68 (5), 1905-1921. <https://doi.org/10.1002/hep.30061>
- Tian, X., Wang, Y., Lu, Y., Wang, W., Du, J., Chen, S., . . . Xiao, Y. (2021). Conditional depletion of macrophages ameliorates cholestatic liver injury and fibrosis via lncRNA-H19. *Cell Death Dis* , 12 (7), 646. <https://doi.org/10.1038/s41419-021-03931-1>
- Tsuchida, T., & Friedman, S. L. (2017). Mechanisms of hepatic stellate cell activation. *Nat Rev Gastroenterol Hepatol* , 14 (7), 397-411. <https://doi.org/10.1038/nrgastro.2017.38>
- Wang, Y., Hong, Y., Zhang, C., Shen, Y., Pan, Y. S., Chen, R. Z., . . . Chen, Y. H. (2019). Picoside II attenuates hyperhomocysteinemia-induced endothelial injury by reducing inflammation, oxidative stress and cell apoptosis. *J Cell Mol Med* , 23 (1), 464-475. <https://doi.org/10.1111/jcmm.13949>

Wen, J., Zhou, Y., Wang, J., Chen, J., Yan, W., Wu, J., . . . Cai, W. (2017). Interactions between Th1 cells and Tregs affect regulation of hepatic fibrosis in biliary atresia through the IFN- $\gamma$ /STAT1 pathway. *Cell Death Differ* , 24 (6), 997-1006.<https://doi.org/10.1038/cdd.2017.31>

Wu, J., Zhang, C., He, T., Zhang, S., Wang, Y., Xie, Z., . . . Cao, L. (2023). Polyunsaturated fatty acids drive neutrophil extracellular trap formation in nonalcoholic steatohepatitis. *Eur J Pharmacol* , 945 , 175618.<https://doi.org/10.1016/j.ejphar.2023.175618>

Zhang, D., Chen, G., Manwani, D., Mortha, A., Xu, C., Faith, J. J., . . . Frenette, P. S. (2015). Neutrophil ageing is regulated by the microbiome. *Nature* , 525 (7570), 528-532.<https://doi.org/10.1038/nature15367>

Zhou, Z., Xu, M. J., Cai, Y., Wang, W., Jiang, J. X., Varga, Z. V., . . . Gao, B. (2018). Neutrophil-Hepatic Stellate Cell Interactions Promote Fibrosis in Experimental Steatohepatitis. *Cell Mol Gastroenterol Hepatol* , 5 (3), 399-413.<https://doi.org/10.1016/j.jcmgh.2018.01.003>

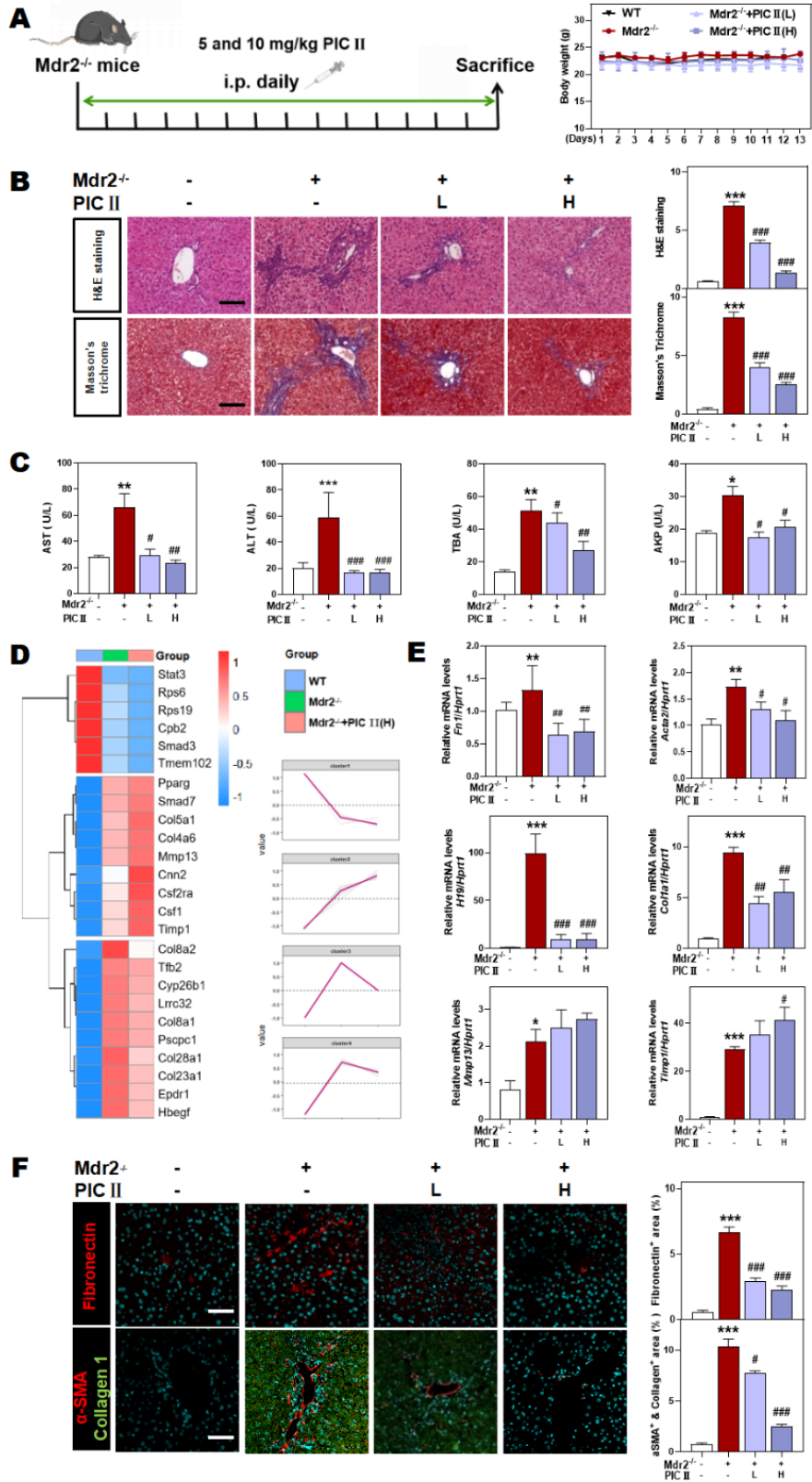


**Figure legends:**

Fig 1. PIC II alleviates hepatic fibrosis and inflammation in *Mdr2*<sup>-/-</sup> mice. **(A)** Flowchart of the animal experiment and body weight changes of different groups. **(B)** Representative images of H & E staining and Masson trichome's staining. Quantifications were performed using *Image J*. Scale bar = 20  $\mu$ m. **(C)** Serum levels of ALT, AST, TBA and AKP. **(D)** The heatmap and clusters of liver fibrosis-related markers. **(E)** Relative mRNA levels of *Fn1*, *Acta2*, *H19*, *Col1a1*, *Mmp13*, and *Timp1* were measured by qPCR and further normalized with *Hprt1*. **(F)** Representative images of immunofluorescence staining for Fibronectin,  $\alpha$ -SMA, and Collagen1 in the liver. Quantifications were performed using *Image J*. Scale bar = 20  $\mu$ m. Statistical significance: \**P* < 0.05, \*\**P* < 0.01, \*\*\**P* < 0.001, compared with the WT group; #*P* < 0.05, ##*P* < 0.01, ###*P* < 0.001, compared with the *Mdr2*<sup>-/-</sup> group (n = 6).

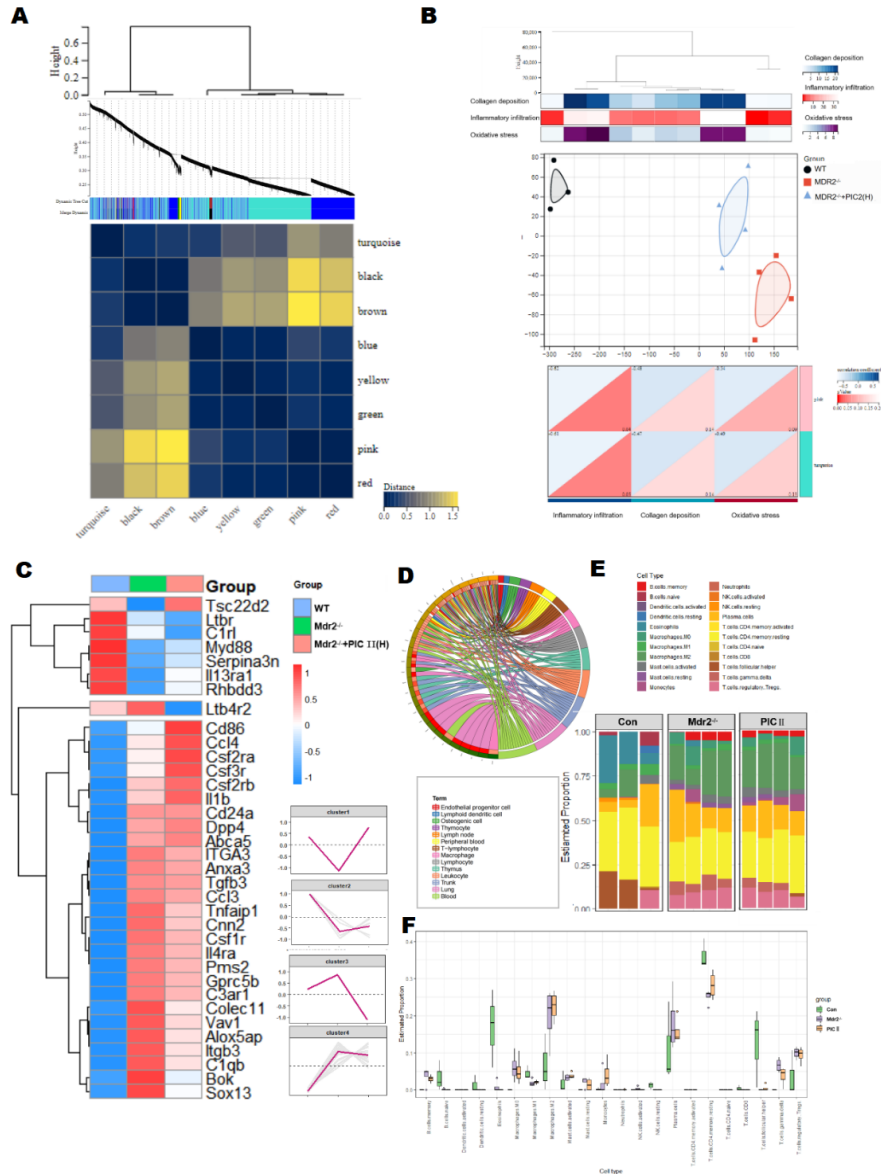


Fig 2. PIC II attenuate hepatic fibrosis *via* improving immune-related DEGs in *Mdr2*<sup>-/-</sup> mice. **(A)** WGCAN plots of RNA-seq analysis. **(B)** Gene co-expression analysis of the inflammatory infiltration, oxidative

stress, and collagen deposition in different groups of mice. (C) The heatmap and clusters of liver fibrosis-related markers. (D) Dominant cells analysis in mice liver. (E) Proportion of immune cell subtypes. (F) CIBERSORT analysis of multiple immune cell subtypes of mice liver.

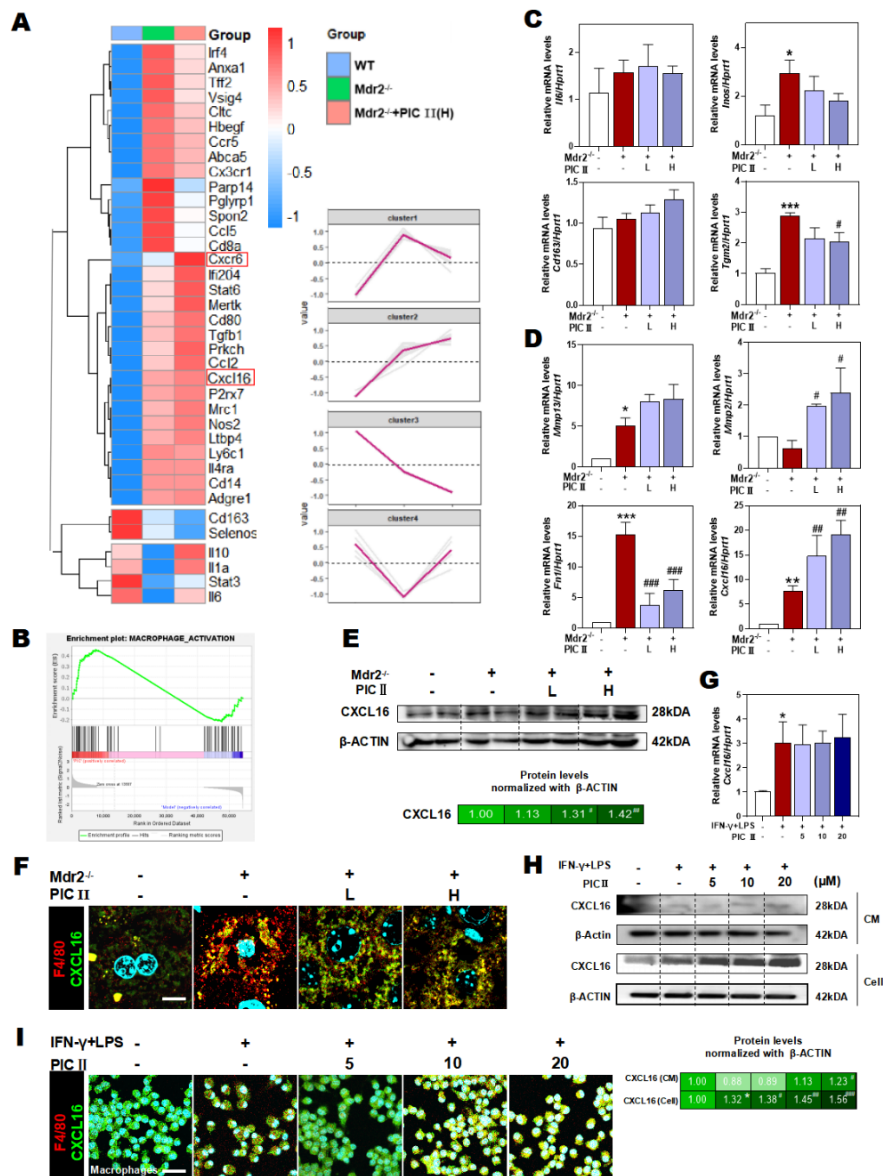


Fig 3. PIC II enhances the function of M1-polarized macrophages and promotes the release of chemokine CXCL16. (A) The heatmap and clusters of M1 type-related macrophage markers. (B) GSEA analysis of M1-polarized macrophage activation. Relative mRNA levels of (C) *Il6*, *Inos*, *Cd163*, *Tgm2*, (D) *Mmp13*, *Mmp2*, *Fn1* and *Cxcl16* in mice liver tissue were measured by qPCR and further normalized with *Hprt1*. (E) The protein levels of CXCL16 were measured by western blot and normalized by  $\beta$ -ACTIN in the mouse liver. Relative mRNA levels of (G) *Cxcl16* in macrophages were measured by qPCR and further normalized with *Hprt1*. (H) The protein levels of CXCL16 in macrophages and derived CM were measured by western blot and normalized by  $\beta$ -ACTIN. Representative images of immunofluorescence staining for F4/80 and CXCL16 (F) in the liver (Scale bar = 20  $\mu$ m) and (I) macrophages (Scale bar = 100  $\mu$ m). Statistical significance:

\* $P < 0.05$ , \*\* $P < 0.01$ , \*\*\* $P < 0.001$ , compared with the control group; # $P < 0.05$ , ## $P < 0.01$ , ### $P < 0.001$ , compared with the model group ( $n = 6$ ).

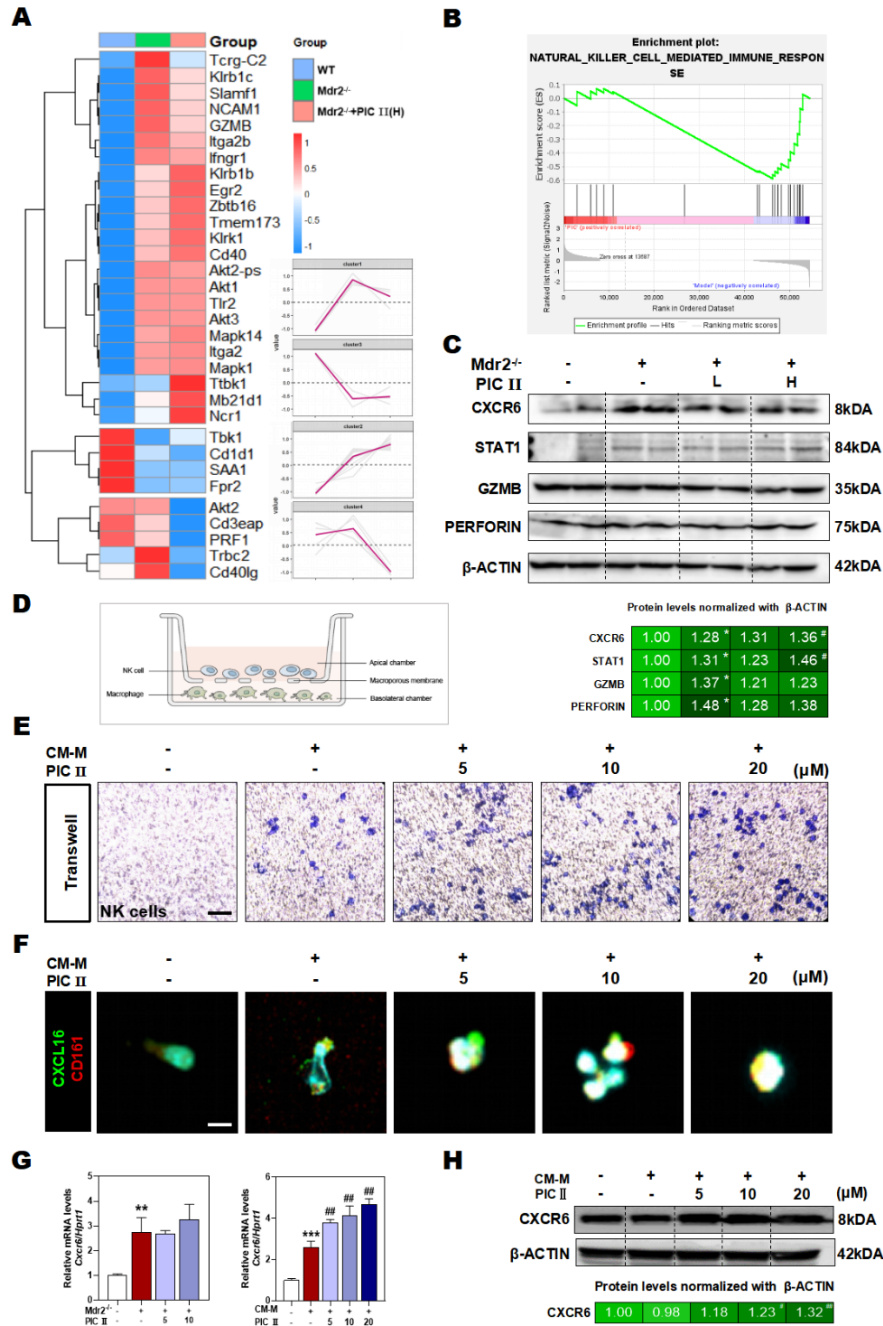


Fig 4. PIC II promotes CXCL16-expressed M1 macrophages to recruit and activate NK cells. (A) The heatmap and clusters of NK cell-related markers. (B) GSEA analysis of NK cell mediated immune response. (C) The protein levels of CXCR6, STAT1, GZMB and PERFORIN were measured by western blot and normalized by  $\beta$ -ACTIN in the mice liver. Quantifications were performed using *Image J*. (D) Schematic of transwell co-culture system of macrophages and NK cells. (E) Representative transwell images of primary NK cells. (F) Representative images of immunofluorescence staining for CD161 and CXCL16 in the primary

NK cells. Scale bar = 100  $\mu\text{m}$ . (G) Relative expression of mRNA levels of *Cxcr6* was measured by qPCR and further normalized with *Hprt1* in the liver and co-cultured NK cells. (H) The protein level of CXCR6 was measured by western blot and normalized by  $\beta$ -ACTIN in the co-cultured NK cells (n = 6). Statistical significance: \* $P < 0.05$ , \*\* $P < 0.01$ , \*\*\* $P < 0.001$ , compared with the control group; # $P < 0.05$ , ## $P < 0.01$ , compared with the model group (n = 6).

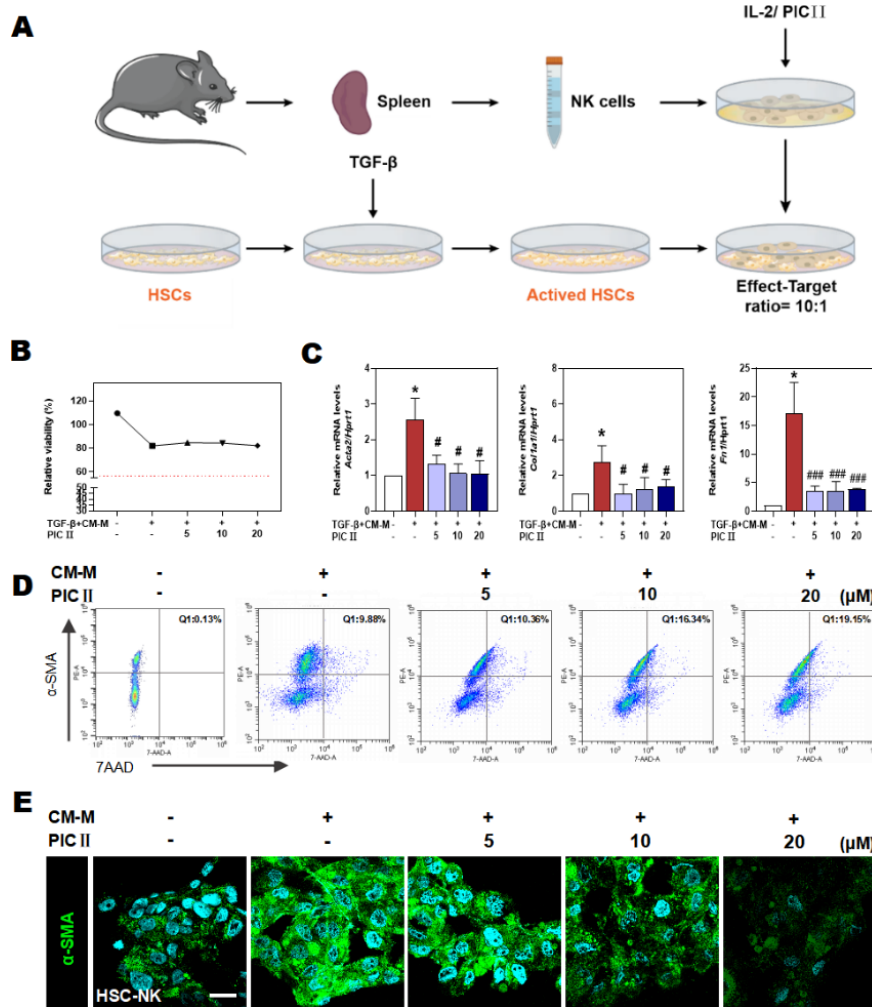


Fig 5. CM secreted by M1-type macrophages containing PIC II facilitated NK cells to promote the apoptosis of HSCs. (A) Flow chart of the primary NK cells co-cultured with HSCs. (B) CCK-8 results. (C) Relative mRNA levels of *Acta2*, *Col1a1* and *Fn1* were measured by qPCR and further normalized with *Hprt1* in the co-culture cells. (D) Flow cytometry of 7-AAD and  $\alpha$ -SMA and (E) representative images of immunofluorescence staining for  $\alpha$ -SMA in the co-culture of primary NK cells and HSCs. Scale bar = 100  $\mu\text{m}$ . Statistical significance: \* $P < 0.05$ , compared with the control group; # $P < 0.05$ , ### $P < 0.001$ , compared with the model group (n = 3).

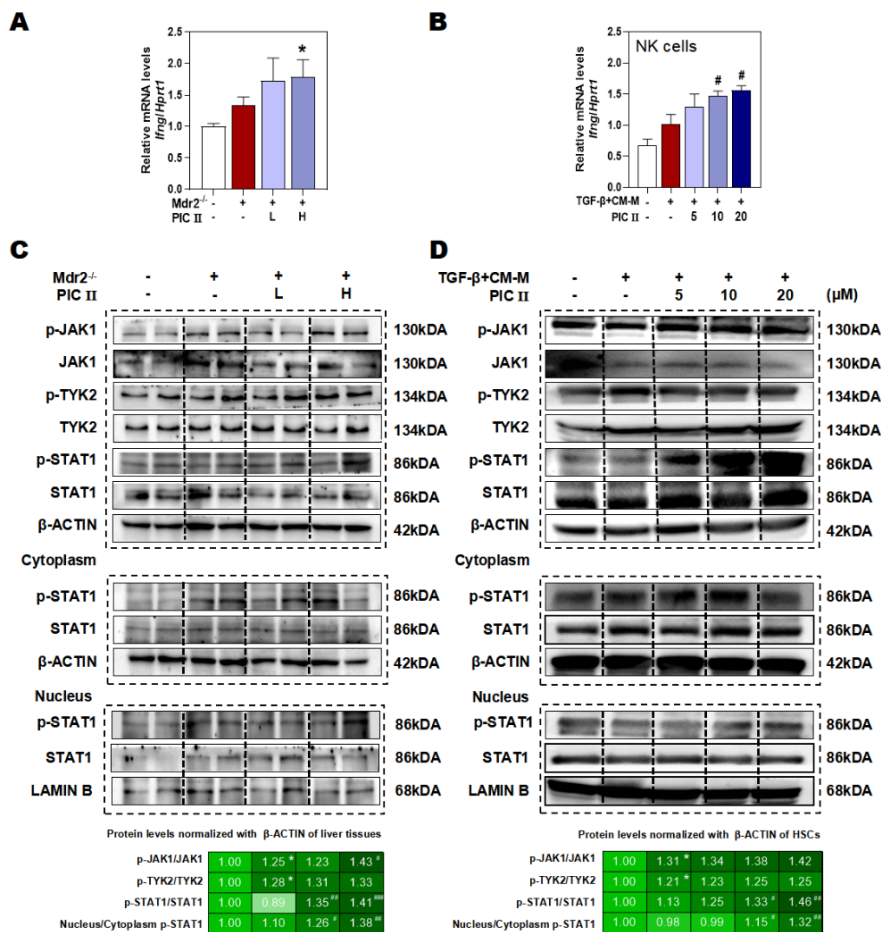


Fig 6. PIC II enhances the killing effects of NK cells on HSCs through IFN- $\gamma$ -Jak1/Tyk2-STAT1 pathway. Relative mRNA levels of *Irf1*- $\gamma$  were measured by qPCR and further normalized with *Hprt1* in (A) mice and (B) primary NK cells. The protein levels of p-JAK1, JAK1, p-TYK2, TYK2, p-STAT1, STAT1 were measured by western blot and normalized by  $\beta$ -ACTIN in the nucleus and cytoplasm of (C) mice liver tissues and (D) co-culture system of NK cells and HSCs. Quantifications were performed using Image J. Statistical significance: \* $P < 0.05$ , compared with the WT group; # $P < 0.05$ , ## $P < 0.01$ , ### $P < 0.001$ , compared with the model group (n = 3).

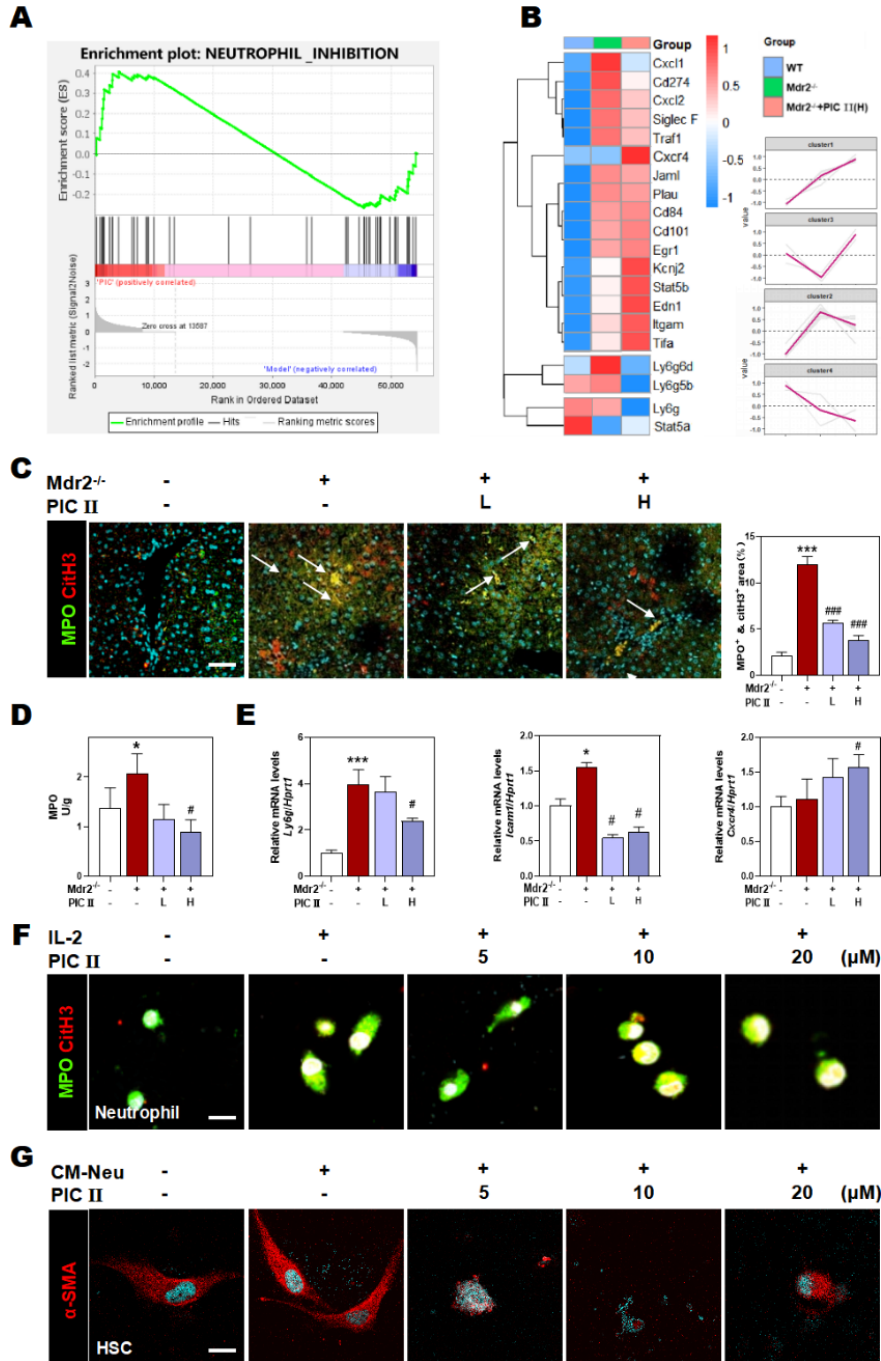


Fig 7. PIC II inhibited the NETs formation and promoted the rupture of aHSCs to alleviate liver fibrosis. (A) GSEA analysis of neutrophil inhibition. (B) The heatmap and clusters of neutrophils-related markers. (C) Representative images of immunofluorescence staining for MPO and CitH3 in the mice liver. Quantifications were performed using Image J. Scale bar = 20 μm. (D) MPO activity. (E) Relative expression of mRNA levels of *Ly6g*, *Icam1* and *Cxcr4* in mice liver were measured by qPCR and further normalized with *Hprt1*. Representative images of immunofluorescence staining for (F) MPO and CitH3 in the primary neutrophils and for (G) α-SMA in the HSCs treated with PIC II and CM-Neu. Scale bar = 100 μm. Statistical significance:

\* $P < 0.05$ , \*\*\* $P < 0.001$ , compared with the control group; # $P < 0.05$ , ### $P < 0.001$ , compared with the model group (n = 3).

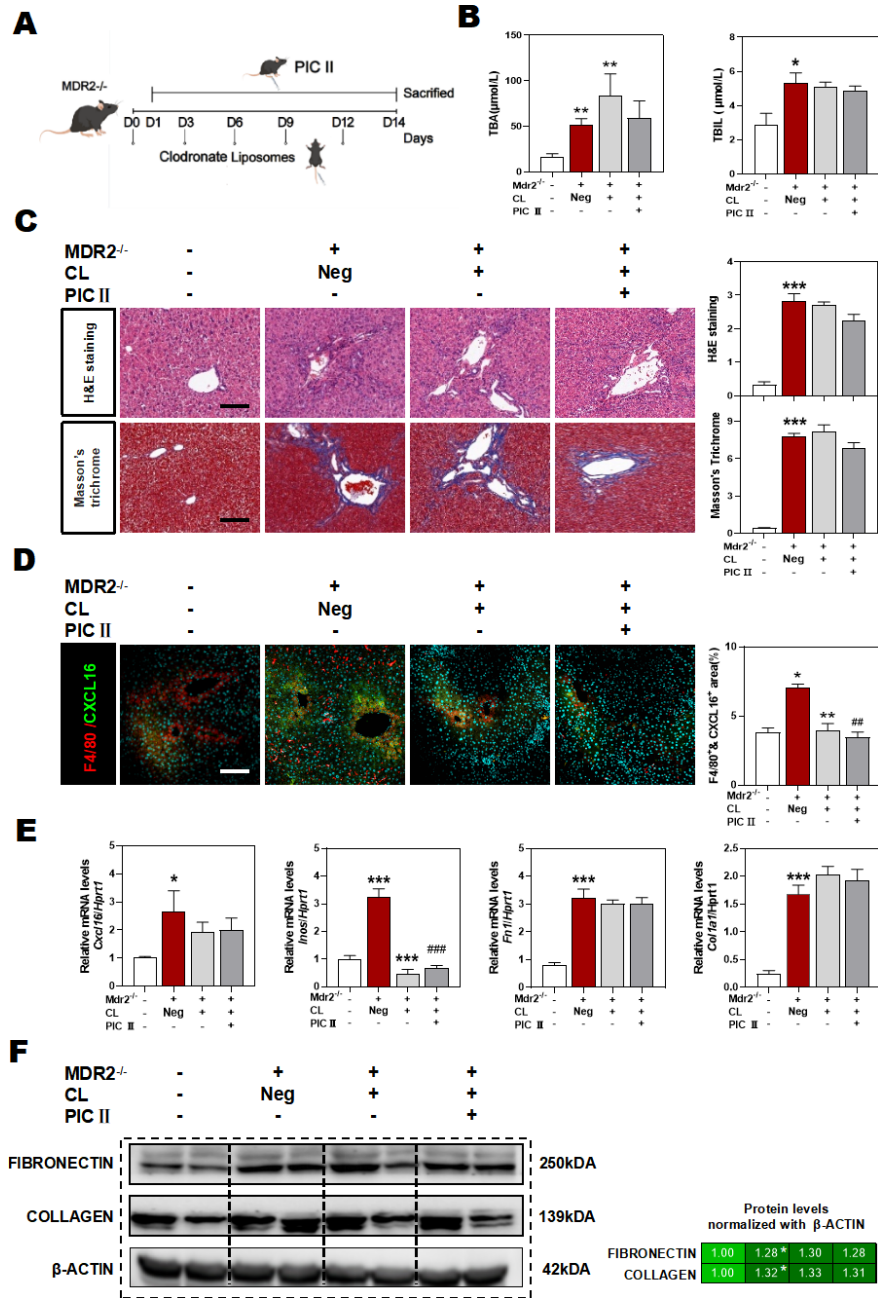


Fig 8. Depletion of macrophages partially neutralizes the anti-fibrotic effect of PIC II. (A) Flowchart of the animal experiment. (B) Serum levels of TBA and TBIL. (C) Representative images of H&E staining and Masson's trichrome staining. Scale bar = 20 μm. (D) Representative images of immunofluorescence staining for F4/80 and CXCL16 in the liver. Scale bar = 20 μm. (E) Relative mRNA levels of *Cxcl16*, *Inos*, *Fn1* and *Col1a1* were measured by qPCR and further normalized with *Hprt1*. (F) The protein levels of FIBRONECTIN and COLLAGEN were measured by western blot and normalized by β-ACTIN in the

liver. Quantifications were performed using Image J. Statistical significance:  $*P < 0.05$ ,  $**P < 0.01$ ,  $***P < 0.001$ , compared with the WT group;  $##P < 0.01$ ,  $###P < 0.001$ , compared with the Mdr2<sup>-/-</sup> group (n = 6).